Biochemical and Biophysical Research Communications 433 (2013) 298–304

Contents lists available at SciVerse ScienceDirect

Biochemical and Biophysical Research Communications

journal homepage: www.elsevier.com/locate/ybbrc

The macroscopic structure of RADA16 peptide hydrogel stimulates monocyte/macrophage differentiation in HL60 cells via cholesterol synthesis

Yasutaka Kakiuchi [a,*], Noritaka Hirohashi [b,c], Kimiko Murakami-Murofushi [b]

[a] Science & Education Center, Ochanomizu University, 2-1-1 Ohtsuka, Tokyo 112-8610, Japan
[b] Department of Biology, Faculty of Science, Ochanomizu University, 2-1-1 Ohtsuka, Tokyo 112-8610, Japan
[c] Oki Marine Biological Station, Education and Research Center for Biological Resources, Faculty of Life and Environmental Science, Shimane University, 194 Kamo, Okinoshima-cho, Oki, Shimane 685-0024, Japan

ARTICLE INFO

Article history:
Received 5 February 2013
Available online 19 March 2013

Keywords:
Three-dimensional culture
Peptide hydrogel
Cell differentiation
Membrane cholesterol

ABSTRACT

Cells can sense physical properties of surrounding 3-dimensional (3D) culture substrata; however, the physiological influences of such sensing are not fully understood. Here, we studied the physiological characteristics and activities of the macroscopic structure of a routinely used 3D culture substrata, the RADA16 self-assembling peptide scaffold. We found that RADA16 exhibited three distinct assembly patterns depending on its concentration, and one of these assemblies, formed with 0.01% (w/v) RADA16, was capable of inducing differentiation of human myelocytic leukemia HL-60 cells into monocytes/macrophages. This activity was largely reduced by destroying the 3D structure of the assembly, suggesting that the assembly intrinsically retained the ability to induce HL-60 differentiation. When cultured in the RADA16 scaffold, HL-60 cells accumulated intracellular cholesterol about 10 times more than normally cultured cells. Both the RADA16 culture and cholesterol loading brought about similar gene expression profiles. These results showed that HL-60 cells can sense the physical properties of the RADA16 scaffold through a mechanism that may involve intracellular pathways of cholesterol synthesis and/or transport.

1. Introduction

Cells often exhibit innate properties when cultured within a 3-dimensional (3D) environment better than when cultured in a 2-dimensional (2D) environment [1]. Based on this finding, a variety of 3D culture substrata have been exploited [2]. It has become clear that 3D cultured cells are influenced by the physical properties of the 3D substrata, such as stiffness or topology of the material surface [3]. These facts suggest that cells are capable of sensing the physical properties of the 3D substrata, at either the microscopic or macroscopic level. However, the detailed molecular mechanisms of such sensing activities have not been elucidated.

Peptide hydrogels represent promising 3D materials for the study of sensing machinery for the following reasons. First, a wide variety of synthetic peptide hydrogels with diverse structures and physical and/or chemical properties have been developed using different combinations and orders of amino acids [4,5]. Second, the structural assemblies of the peptide hydrogels are able to be manipulated on a large scale (μm order) [6,7] as well as a small scale (sub-nm order) [8] depending on the conditions and peptide species.

Here, we evaluated a peptide hydrogel, 16-mer peptide RADA16 (RADARADARADARADA), according to the intrinsic physical properties of the hydrogel [9] and examined its ability to induce cell differentiation.

2. Materials and methods

2.1. Chemicals

RADA16 peptide was supplied by 3D Matrix Japan Co., Ltd. (Tokyo, Japan) as a 1% solution in water. Hydroxypropyl-β-cyclodextrin (CD) was provided by Nihon Shokuhin Kako Co., Ltd. (Tokyo, Japan). Congo red, cholesterol, methylcellulose (25 cp), and TPA were purchased from Wako Chemical (Tokyo, Japan). The RGDS peptide was purchased from Sigma Chemicals (Tokyo, Japan).

2.2. Cell line, culture conditions, and 3D environment analysis

Human promyelocytic leukemia cells (HL-60 cells) were obtained from the Riken Cell Bank (RCB0041). Cells were grown in RPMI-1640 (Nissui, Tokyo, Japan) supplemented with 10% heat-inactivated fetal bovine serum (S1610, Biowest, Florida, USA), pas-

Abbreviations: CD, hydroxypropyl-β-cyclodextrin; FT, fourier transformation.

* Corresponding author. Fax: +81 3 5978 5471.
E-mail address: kakiuchi.yasutaka@ocha.ac.jp (Y. Kakiuchi).

0006-291X/$ - see front matter © 2013 Elsevier Inc. All rights reserved.
http://dx.doi.org/10.1016/j.bbrc.2013.02.105

saged every 4 days at 0.5×10^5 cells/mL. For cell culture assays, cells were cultured in 24-well cell culture plates (3047, Becton Dickinson, Tokyo, Japan) at 1×10^6 cells/mL. For 3D culture assay, cells were recovered by centrifugation (150×*g* for 3 min), washed with 10% sucrose in water, and resuspended in an appropriate volume of 10% sucrose. The cell solution was mixed with an equal volume of RADA16 solution, which was diluted beforehand to a given concentration with 10% sucrose. Four hundred microliters of the mixture was poured into a well of the culture plate, and 1 mL of RPMI-1640 medium with 10% FBS was immediately applied onto the mixture. Thus, the final concentration of FBS was 7.1% in the 3D culture, and the concentration of FBS in the control culture was adjusted to the same concentration. The macroscopic structure of the RADA16 gel was ascertained by microscopy after staining with 10 μg/mL Congo red. To destroy the macroscopic gel structure, 1.4 mL of the culture setup (400 μL of gel and 1 mL of culture media) was gently pipetted four times with a pipetter set at 800 μL. During the culture assay, this manipulation was repeated every 12 h. Pipetting was also performed for cells in the control culture. In order to avoid the formation of cell clusters, cells were recovered 48 h after the onset of culture and subjected to mRNA extraction. For all assays, cell viability was evaluated by trypan blue exclusion.

2.3. Immunofluorescent staining

After rinsing with PBS, 100 μL of the cell solution was dropped in 1 mL ice-cold 0.5% paraformaldehyde in PBS. After 20 min, fixation was arrested by adding 50 μL of 1 M NH_4Cl. After rinsing with PBS, 100 μL of the cell suspension was added to 5 μL of anti-CD14 antibodies conjugated with R-phycoerythrin (P5435: clone UCHM-1; Sigma).

2.4. Flow cytometry

Flow cytometry was performed for the measurement of cell volume (electronic cell volume), side scatter intensity, and fluorescence intensity using a microtiter plate-based flow cytometer (Cell Lab Quanta SC, Beckman Coulter, Tokyo, Japan) according to the manufacturer's instructions. One milliliter containing at least 5×10^5 living cells or immunostained fixed cells was applied to the analysis.

2.5. Quantitative RT-PCR

Expression levels of mRNAs were determined by fluorescent real-time PCR. After removal of the RADA16 peptide by centrifugation at 120×*g*, total RNA was extracted from the cultured cells using an RNA extraction kit (MagExtractor RNA, Toyobo, Tokyo, Japan), and cDNA was synthesized from 1 to 4 mg of total RNA using a cDNA synthesis kit (Omniscript RT, Qiagen, Tokyo, Japan). Real-time PCR was performed with Premix Ex-Taq (Takara, Tokyo, Japan) on a Prism 7300 instrument (ABI, Tokyo, Japan) using the following conditions: preheat at 50.0 °C for 2 min, hot start at 95.0 °C for 20 s, and 40 cycles of denaturation at 95.0 °C for 5 s and annealing at 60.0 °C for 31 s. The relative amount of cDNA was determined by the standard curve method, followed by normalization to the expression of five internal control genes (glyceraldehyde 3-phosphate dehydrogenase, hypoxanthine phosphoribosyltransferase 1, succinate dehydrogenase complex, subunit A, TATA box binding protein, and 14-3-3 zeta) by the geometric averaging method [10]. Real-time PCR results were expressed as fold change ($2^{-\Delta\Delta CT}$) relative to the expression level in the untreated control. Primer sequences used in the PCR procedure will be provided upon request.

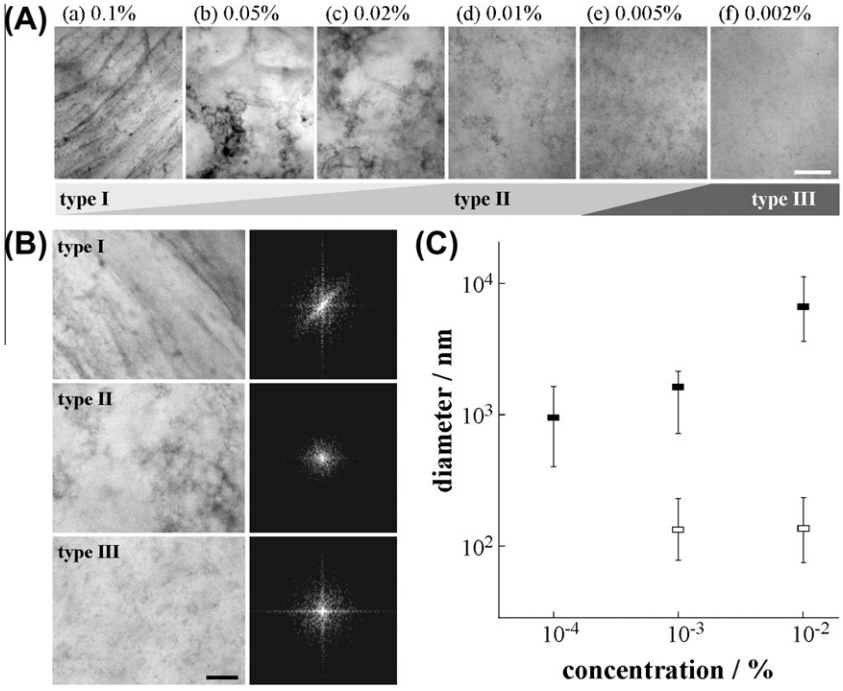

Fig. 1. Macroscopic structure of RADA16 hydrogels with different RADA16 concentrations. (A) Microscopic images of RADA16 gels with concentrations at 0.1% (a), 0.05% (b), 0.02% (c), 0.01% (d), 0.005% (e), and 0.002% (f). The bar represents 200 μm. For type I, type II, and type III structures of RADA16, see Results and discussion. The horizontal bar below the images indicates observed types of RADA16 assembly at each concentration. (B) Representative microscopic images (left) and corresponding 2-dimensional Fourier transformation (right) of type I, II, and III structures. The bar represents 100 μm. (C) Particle size distribution of RADA16 with concentrations at 0.0001%, 0.001%, and 0.01% prepared with (filled boxes) or without (open boxes) NaCl. Top and bottom of bars represent the 25th and 75th percentiles, respectively, and boxes within the bars represent the median.

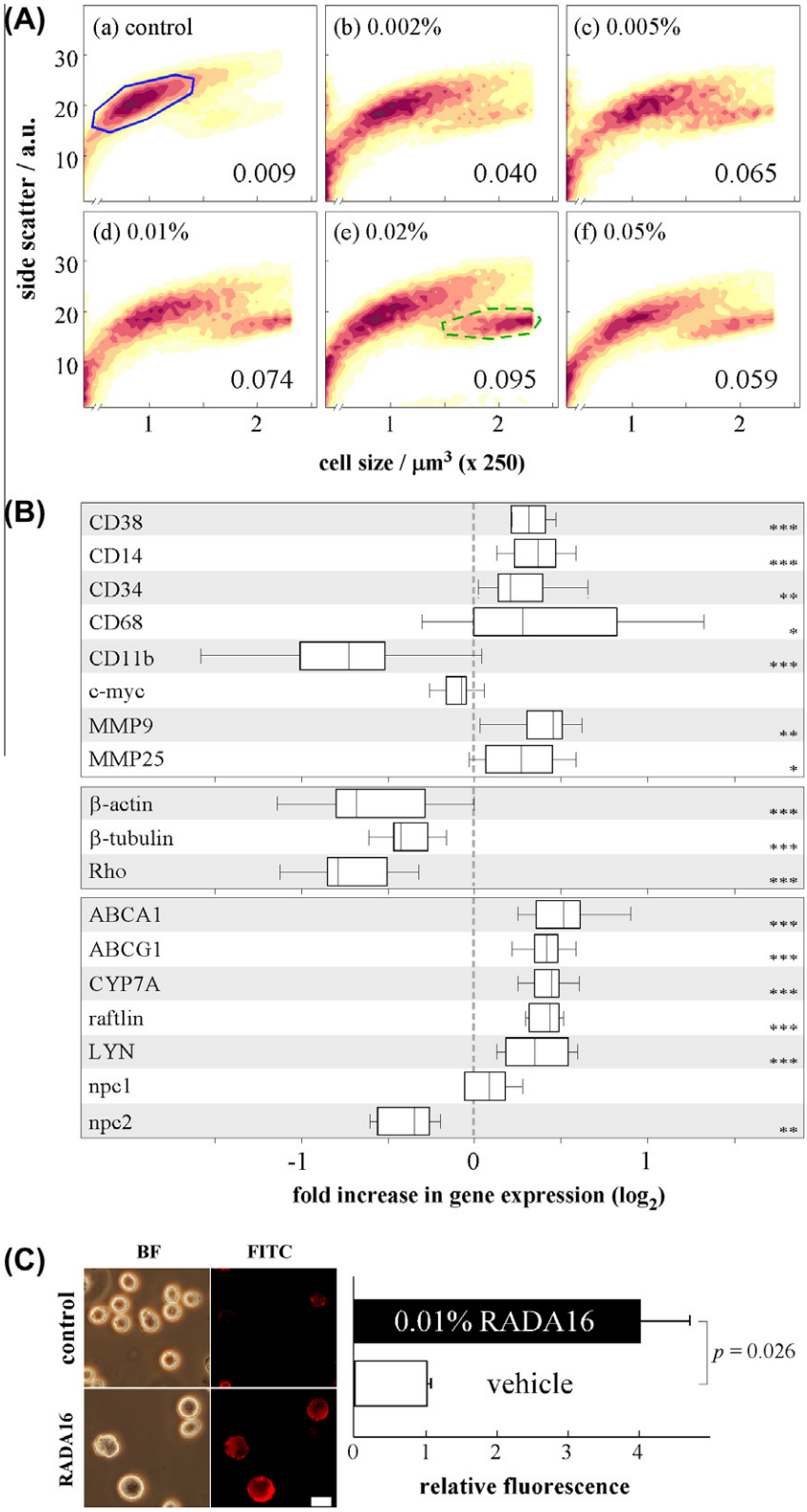

Fig. 2. Flow cytometric and gene expression analyses of HL-60 cells cultured in RADA16. (A) Flow cytometric analysis of cells cultured for 20 days in RADA16 at 0–0.05% (w/v) concentrations. The intensity of side scatter light is plotted against cell size for each cell. The color density represents the cell number. Circles in (a) and (e) indicate the defined regions of small- and large-sized cells, respectively. The ratio of the number of large-sized cells (L) to the number of small-sized cells (S) is indicated (L/S ratio) at right-bottom corner in each panel ($n = 4$). (B) Gene expression profile for cells cultured in RADA16 gel. Relative gene expression levels in RADA16-cultured cells are shown in the box plot for selected genes related to blood cell differentiation (eight genes in the upper panel), cell cytoskeleton (three genes in the middle panel), and cholesterol metabolism (seven genes in the lower panel). Relative gene expression levels are shown in log2 scale as the fold increase. Boxes of each bar are limited by the first and third quartiles; lines within the boxes represent medians; T-bars represent minima and maxima.*, **, and *** represent $P < 0.05$, 0.01, and 0.001, respectively. (C) Cell surface expression of CD14 after 4 days culture with 0.01% RADA16. Left, bright-field (BF) and fluorescence (FITC) microscopy of cells cultured for 4 days in control conditions (upper) and with RADA16 hydrogel (lower). The bar represents 10 μm. Right, relative fluorescence (FITC) intensity of the cells cultured with or without RADA16 scaffold.

2.6. Quantification of cellular cholesterol

Total cellular cholesterol content was quantified with the Cholesterol/Cholesteryl Ester Quantification Kit (K603, BioVision, CA, USA), as described in the manufacturer's protocol, using a luminescent image analyzer (LAS-3000, Fujifilm, Tokyo, Japan) with a 605 nm interference filter.

2.7. Cholesterol loading

Cholesterol was incorporated into CD molecules to form cholesterol-CD complexes and dosed to cells according to a previously described method [11]. Fourteen microliters of 100 mM cholesterol solution (1.4 μmol) in chloroform was dried at 50 °C to form a thin-film in a 1.5 mL tube. Then, 140 μL of 100 mM CD and 860 μL of 10% FBS in RPMI-1640 medium was added, and the mixture was sonicated in ice/water with an ultrasonic bath (3200, Branson, Tokyo, Japan) for 30 min. The cholesterol solution was then mixed with 400 μL of the cell solution to obtain the final concentrations of 1 mM cholesterol and 10 mM CD. Cells were incubated for 15 h at 37.8 °C and then recovered to examine the mRNA expression levels of target genes.

2.8. Laser diffraction particle size analysis

Ten milliliters of RADA16 solution was prepared at various concentrations with or without 100 mM NaCl, and particle size was analyzed using a submicron particle size analyzer (LS 13320, Beckman Coulter, Tokyo, Japan) by means of a dynamic light scattering at 25 °C. Measurements were performed from 1.0 nm to 100 μm (43 steps). All measurements were conducted in triplicate.

2.9. Two-dimensional Fourier analysis

Bright field microscopy for Congo red-stained RADA16 was subjected to 2D Fourier transformation (FT) using ImageJ software (version 1.45, National Institute of Health, MD, USA).

2.10. Statistics

Statistical significance was determined by analysis of variance (ANOVA; $P < 0.05$).

3. Results and discussion

3.1. Macroscopic structure of diluted RADA16

RADA16 formed several macroscopic structures in the concentration range of 0.001–0.1% (Fig. 1A). We first classified these hydrogels into three types of structures (Fig. 1B, Supplementary Fig. 1), i.e., type I showing membranous structure with regular thickness, type II showing structural flexibility and heterogeneity in peptide density, and type III showing uniformly dispersed particles. Two-dimensional FT also distinguished these structures from each other. In type I, the FT was distributed asymmetrically, representing the structure's orientation, and FT appeared with a smaller halo radius in type II structures than in type III structures, suggesting that the structure of type III was larger than that of type II. Types I, II, and III appeared as dominant species in the concentration ranges around 0.1%, 0.02%, and 0.002%, respectively. The structural differences between types II and III were determined by laser diffraction analysis (Fig. 1C). In the absence of cations, the median particle diameter of RADA16 was nearly constant around 100 nm, regardless of the concentration. In contrast, in the presence of cations necessary for gelation of RADA16, the median particle diameter at 0.01% (6.5 μm) was approximately four times greater than that at 0.001% (1.7 μm). The particle size observed in diluted RADA16 solution resembled that of globular aggregates of RADA16 in acidic conditions or at high temperatures [6]. EAK16-II, another 16 mer (AEAEAKAKAEAEAKAK) peptide, transforms its assembled form from fibrous to globular depending on the peptide concentration around 0.01% (w/v) [7]. It is possible that similar dynamics may occur during the molecular assembly of RADA16.

3.2. Differentiation of HL-60 cells in RADA16

We next studied the effects of RADA16 concentration on the culture of HL-60 cells, which are known to differentiate into either myelocytic (monocytes and macrophages) or granulocytic (neutrophils) cell lineages upon stimulation with several chemical stimuli [12]. After 3 weeks culture of HL-60 cells in several concentrations of RADA16, the cells formed scattered clusters (Supplementary Fig. 2A). Flow cytometric analyses (Fig. 2A) revealed that these scattered clusters contained major (solid circle in (a)) and minor (broken circle in (e)) cell populations distinguished by cell size and side scattering. The proportion of the minor cell subpopulation (calculated by the ratio of large to small cell subpopulations; L/S) increased as gel concentration increased until 0.02% and thereafter decreased by 38% at 0.05%. The characteristics of increased cell size

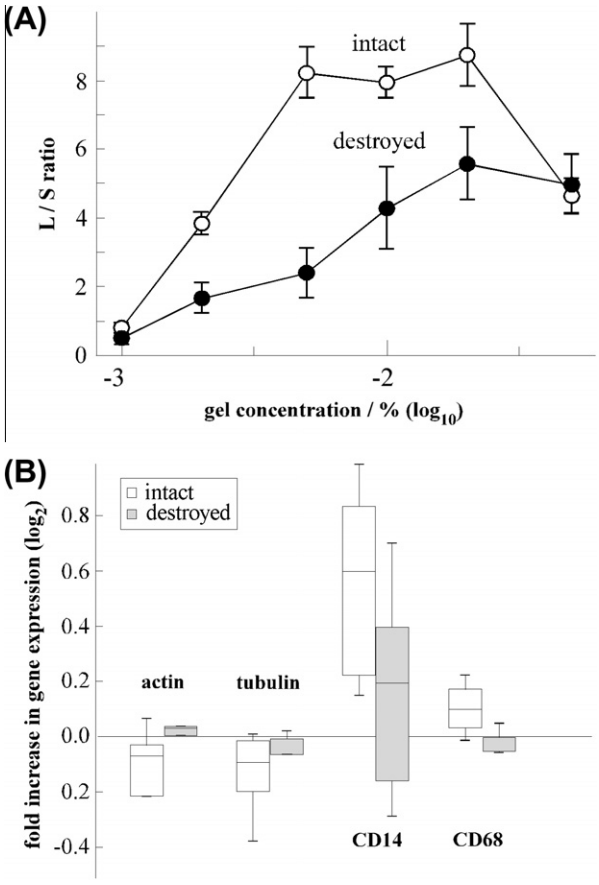

Fig. 3. Effects of destroying the macroscopic gel structure on cellular properties. (A) The relationship between the L/S ratio of cells cultured for 20 days and the concentration of intact (open) and destroyed (close) RADA16. For L/S ratio, see Fig. 2. *P* values are 0.50 (0.001%), 0.18 (0.002%), 0.11 (0.005%), 0.30 (0.01%), 0.39 (0.02%), and 0.89 (0.05%). (B) Relative expression levels of *β-actin*, *β-tubulin*, *CD14*, and *CD68* of cells cultured for 48 h in the intact (open) and destroyed (gray) RADA16. The expression levels are shown as described in Fig. 2. *P* values are 0.17 (*actin*), 0.16 (*tubulin*), 0.11 (*CD14*), and 0.12 (*CD68*).

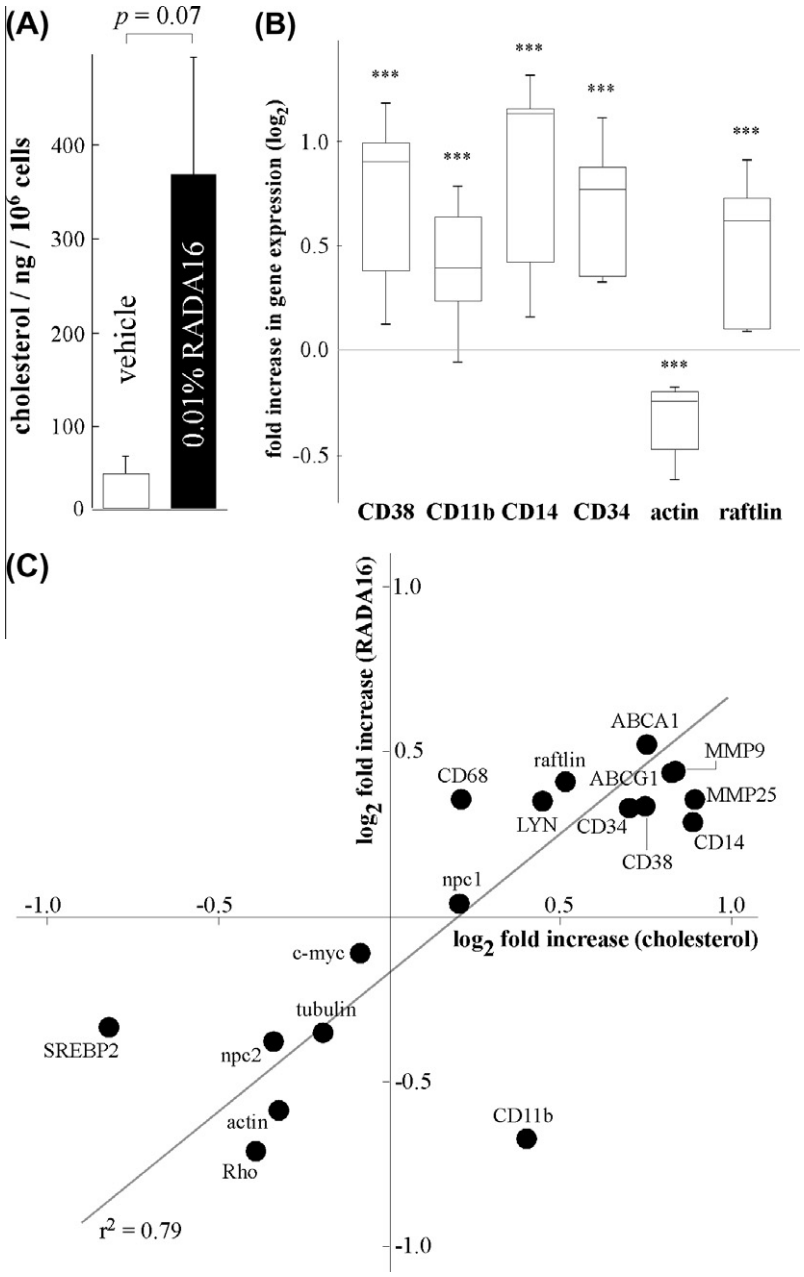

Fig. 4. Intracellular cholesterol levels in RADA16-cultured cells and gene expression profiles of cholesterol-exposed cells. (A) Intracellular free cholesterol level within the cells cultured for 24 h in 0.01% RADA16. (B) Relative expression levels of genes within the cells loaded with 140 μM cholesterol. The expression levels are shown as described in Fig. 2. $^{***}P < 0.001$. (C) Correlations of gene expression profiles for cells exposed to 140 μM cholesterol (abscissa) and those cultured in 0.01% RADA16 (ordinate).

[13] and decreased side scatter [14] suggested that the subpopulation was differentiated into monocyte/macrophage-like cells.

To confirm this prediction, quantitative RT-PCR was performed to investigate the expression levels of genes relevant to monocyte/macrophage differentiation (Fig. 2B). When the cells were cultured in 0.01% RADA16, they underwent differentiation without any significant suppression of cell proliferation (Supplementary Fig. 2B). We found that *CD14* [15–17], *CD38* [18], *CD68* [19], *MMP-9* [20], and *MMP-25* [21], typical markers of monocyte/macrophage differentiation, were upregulated, supporting our prediction. However, the expression profiles of several other genes, including *CD11b*, *CD34*, and *raftlin*, were inconsistent with those in typical monocytes/macrophages as follows. *CD11b* is typically upregulated during monocyte differentiation and is therefore used as a myeloid differentiation marker [22]. In RADA16 cultures, however, it was strongly downregulated (−0.7, $P < 0.001$). *CD34* and *raftlin* are known to be expressed specifically in endothelial cells [23] and B cells [24], respectively, but were both upregulated in RADA16 cultures. A recent study reported the presence of CD34-positive HL-60 subpopulations that proliferated in methyl cellulose culture [25]. The cell surface expression of CD14 was also confirmed by immunofluorescence (Fig. 2C). However, we could not verify the superoxide anion production of cells by NBT assay (data not shown), suggesting the possibility that functional differentiation of HL-60 cells to macrophages remained incomplete.

Our results indicated that the ability of RADA16 to induce monocyte/macrophage differentiation was attributable to the chemical nature or structural features of RADA16. To distinguish between these two possibilities, cell culture was performed with intact RADA16 gel or RADA16 gel destroyed by pipetting (see

Materials and methods). Pipetting itself did not affect gene expression in HL-60 cells (data not shown), but this manipulation largely destroyed the macroscopic assembly of the peptide, and the cells were not retained suspended but sank to the bottom of the culture well (data not shown). Following pipetting, the ratio of larger cells to smaller cells (L/S) was decreased by up to 71% (Fig. 3A), and variations in the mRNA levels of the marker genes were decreased (Fig. 3B), suggesting that the differentiation of HL-60 cell to monocytes/macrophages was suppressed. Since gentle pipetting itself unlikely alters the chemical and/or molecular nature of RADA16 peptides, these results suggested that the induction of monocyte/macrophage differentiation by RADA16 was attributable to the macroscopic structure of the hydrogel.

3.3. Intracellular cholesterol accumulation within RADA16-cultured cells

Raftlin is a marker of membrane lipid raft [26], and cholesterol is the major lipid component of rafts. Thus, we next investigated mRNA expression for genes related to cholesterol metabolism and transport (Fig. 2B). *ABCA1*, *ABCG1* [27–29], and *lyn* [30], which are known to exhibit increased mRNA expression during monocyte/macrophage differentiation, were upregulated in RADA16-cultured cells. *CYP7A*, a liver-specific gene that converts cholesterol to bile acid [31], was also upregulated (0.46, $P < 0.001$). More interestingly, we observed downregulation of *npc2* (−0.3, $P < 0.01$). NPC2 is responsible for intracellular cholesterol transport, and the impairment of its function results in elevated endosomal cholesterol levels [32]. Indeed, the amount of intracellular free cholesterol of in RADA16 gel-cultured cells was 10 times greater than that in cells cultured under normal conditions for 24 h (Fig. 4A).

Cholesterol administration is one of the major cues for the induction of monocyte/macrophage differentiation [33,34]. In order to verify whether cholesterol-stimulated signaling was relevant to cell differentiation in RADA16 cultures, we studied the effects of free cholesterol loading by exposing cells to the CD/cholesterol complex without RADA16. With low-dose loading (70/1 molar ratio of CD/cholesterol), no significant change was observed in the expression levels of the genes tested (data not shown), but with high-dose loading (10/1), several genes were up- or downregulated (Fig. 4B). Interestingly, cells cultured in RADA16 and those exposed to cholesterol both exhibited similar changes in their gene expression profiles, including changes in *CD34*, *raftlin*, and *npc2*, which are not typical marker genes for monocyte/macrophage differentiation (Fig. 4C); only *CD11b* exhibited an opposite change among genes tested, i.e., its expression was reduced in RADA16 cultures. The correlation coefficient R^2 of these data was 0.79 when *CD11b* was excluded. Thus, the signaling pathway involved in RADA16 scaffold-induced macrophage differentiation may be, at least in part, associated with cholesterol accumulation. However, a striking difference was seen in cell viability, i.e., loading with high-dose cholesterol was severely toxic for cells and resulted in a dramatic reduction in cell viability within 20 h (<50%) compared to culture in the RADA16 scaffold for 48 h (>95%). Cholesterol administration is known to induce the apoptotic pathway in cells [35]; therefore, this pathway may remain quiescent in cells cultured in the RADA16 scaffold.

Cholesterol appears to be the key factor in RADA16-induced differentiation, as shown in Fig. 4. In this view, *npc2* may play a pivotal role, as the downregulation of the *npc2* gene independently provokes cellular cholesterol accumulation. Then, how is *npc2* expression regulated? We speculate that CD11b, whose expression profile was opposite in cells cultured with RADA16 and those exposed to cholesterol loading, may be the initial sensor for RADA16 assembly. CD11b forms a heterodimer with CD18, giving αMβ2 integrin, which regulates the expression of the *FoxP1* transcription factor through clustering; this transcription factor is known to function in monocyte differentiation [36]. Martino et al. reported a direct relationship between cholesterol and CD11b, in which cell surface CD11b levels are downregulated in peripheral blood mononuclear cells in patients with hypercholesterolemia, and these levels are negatively correlated with total cholesterol concentration [37]. The causal relationship between these two components is not clear; however, the macro- and microscopic structure of RADA16 indeed does affect cell-substrate interactions, which may involve certain modifications of the assembly of cell surface proteins, possibly including the CD11b integrin. To elucidate the detailed mechanism of RADA16-induced differentiation, future studies should address the fine structure and physicochemical nature of type II assemblies, as well as the molecular mechanisms through which cells can distinguish type II assemblies from other types of RADA16 3D matrices.

Acknowledgments

This work was supported by JSPS KAKENHI, Grant No. 24657151 to Y.K. We would like to thank Editage for providing editorial assistance.

Appendix A. Supplementary data

Supplementary data associated with this article can be found, in the online version, at http://dx.doi.org/10.1016/j.bbrc.2013.02.105.

References

[1] F. Pampaloni, E.G. Reynaud, E.H.K. Stelzer, The third dimensions bridges the gap between cell culture and live tissue, Nat. Rev. Mol. Cell Biol. 8 (2007) 839–845.
[2] J. Lee, M.J. Cuddihy, N.A. Kotov, Three-dimensional cell culture matrices: state of the art, Tissue Eng. Part B 14 (2008) 61–86.
[3] M.M. Stevens, J.H. George, Exploring and engineering the cell surface interface, Science 310 (2005) 1135–1138.
[4] P. Kumar, V. Pillary, G. Modi, et al., Self-assembling peptides: implications for patenting in drug delivery and tissue engineering, Recent Pat. Drug Deliv. Formul. 5 (2011) 24–51.
[5] J. Kopeček, J. Yang, Smart self-assembled hybrid hydrogel biomaterials, Angew. Chem. Int. Ed. 51 (2012) 7396–7417.
[6] Z. Ye, H. Zhang, H. Luo, et al., Temperature and pH effects on biophysical and morphological properties of self-assembling peptide RADA16-I, J. Pept. Sci. 14 (2008) 152–162.
[7] S. Jun, Y. Hong, H. Imamura, et al., Self-assembly of the ionic peptide EAK16: the effect of charge distributions on self-assembly, Biophys. J. 87 (2004) 1249–1259.
[8] S. Jang, J.-M. Yuan, J. Shin, et al., Energy landscape associated with the self-aggregation of an alanine-based oligopeptide $(AAKA)_4$, J. Phys. Chem. B 113 (2009) 6054–6061.
[9] H. Yokoi, T. Kinoshita, S. Zhang, Dynamic reassembly of peptide RADA16 nanofiber scaffold, Proc. Natl. Acad. Sci. USA 102 (2005) 8414–8419.
[10] J. Vandesompele, K.D. Preter, F. Pattyn, et al., Accurate normalization of real-time quantitative RT-PCR data by geometric averaging of multiple internal control genes, Genome Biol. 3 (2002) 0034.1–0034.11.
[11] A.E. Christian, M.P. Haynes, M.C. Phillips, et al., Use of cyclodextrins for manipulating cellular cholesterol content, J. Lipid Res. 38 (1997) 2264–2272.
[12] G.D. Birnie, The HL60 cell line: a model system for studying human myeloid cell differentiation, Br. J. Cancer 58 (Suppl. 9) (1988) 41–45.
[13] K. Yun, H. Sugihara, Cell differentiation and cell cycle effects on human promyelocytic leukemia cells induced by 12-*O*-tetradecanoylphorbol-13-acetate, Lab. Invest. 54 (1986) 336–344.
[14] M. Daigneault, J.A. Preston, H.M. Marriott, et al., The identification of markers of macrophage differentiation in PMA-stimulated THP-1 cells and monocyte-derived macrophages, PLoS One 5 (2010) e8668.1–e8668.10.
[15] D.E. Zhang, C.J. Hetherington, D.A. Gonzalez, et al., Regulation of CD14 expression during monocytic differentiation induced with 1 alpha, 25-dihydroxyvitamin D3, J. Immunol. 153 (1994) 3276–3284.
[16] C. Li, Y. Wang, L. Gao, et al., Expression of Toll-like receptor 2 and 4 and CD14 during differentiation of HL-60 cells induced by phorbol 12-myristate 13-acetate and 1-, 25-dihydroxy-vitamin D3, Cell Growth Differ. 13 (2002) 27–38.
[17] T.T. Tuomisto, M.S. Riekkinen, H. Viita, et al., Analysis of gene and protein expression during monocyte-macrophage differentiation and cholesterol loading–– cDNA and protein array study, Atherosclerosis 180 (2005) 283–291.

[18] T. Musso, S. Deaglio, L. Franco, et al., CD38 expression and functional activities are up-regulated by IFN- on human monocytes and monocytic cell lines, J. Leukoc. Biol. 69 (2001) 605–612.
[19] Y.Y. Chen, H.M. Chang, Antiproliferative and differentiating effects of polysaccharide fraction from fu-ling (*Poria cocos*) on human leukemic U937 and HL-60 cells, Food Chem. Toxicol. 42 (2004) 759–769.
[20] B. Xie, A. Laouar, E. Huberman, Fibronectin-mediated cell adhesion is required for induction of 92 kDa type IV collagenase/gelatinase (MMP-9) gene expression during macrophage differentiation, J. Biol. Chem. 273 (1998) 11576–11582.
[21] A. Bar-Or, R.K. Nuttall, M. Duddy, et al., Analyses of all matrix metalloproteinase members in leukocytes emphasize monocytes as major inflammatory mediators in multiple sclerosis, Brain 126 (2003) 2738–2749.
[22] A.G. Rosmarin, S.C. Weil, G.L. Rosner, et al., Differential expression of CD11b/CD18 (Mo1) and myeloperoxidase genes during myeloid differentiation, Blood 73 (1989) 131–136.
[23] H.B. Wood, G. May, L. Healy, et al., CD34 expression patterns during early mouse development are related to modes of blood vessel formation and reveal additional sites of hematopoiesis, Blood 90 (1997) 2300–2311.
[24] K. Saeki, Y. Mimura, D. Aki, et al., The B cell-specific major raft protein, Raftlin, is necessary for the integrity of lipid raft and BCR signal transduction, EMBO J. 22 (2003) 3015–3026.
[25] K. Kuranda, C. Berthon, F. Leprêtre, et al., Expression of CD34 in hematopoietic cancer cell lines reflects tightly regulated stem/progenitor-like state, J. Cell. Biochem. 112 (2011) 1277–1285.
[26] K. Saeki, S. Fukuyama, T. Ayada, et al., A major lipid raft protein raftlin modulates T cell receptor signaling and enhances Th17-mediated autoimmune responses, J. Immunol. 182 (2009) 5929–5937.
[27] G. Schmitz, W.E. Kaminski, M. Porsch-Özcürümez, et al., ATP-binding cassette transporter A1 (ABCA1) in macrophages: a dual function in inflammation and lipid metabolism?, Pathobiology 67 (1999) 236–240
[28] A.E. Bortnick, G.H. Rothblat, G. Stoudt, et al., The correlation of ATP binding cassette one mRNA levels with cholesterol efflux from various cell types, J. Biol. Chem. 275 (2000) 28634–28640.
[29] J. Klucken, C. Büchler, E. Orsó, et al., ABCG1 (ABC8), the human homolog of the *Drosophila* white gene, is a regulator of macrophage cholesterol and phospholipid transport, Proc. Natl. Acad. Sci. USA 97 (2000) 817–822.
[30] K. Katagiri, T. Katagiri, Y. Koyama, et al., Expression of src family genes during monocytic differentiation of HL-60 cells, J. Immunol. 146 (1991) 2701–2707.
[31] R.A. Davis, J.H. Miyake, T.Y. Hui, et al., Regulation of cholesterol-7 alphahydroxylase: BARElY missing a SHP, J. Lipid Res. 43 (2002) 533–543.
[32] R.E. Infante, M.L. Wang, A. Radhakrishnan, et al., NPC2 facilitates bidirectional transfer of cholesterol between NPC1 and lipid bilayers, a step in cholesterol egress from lysosomes, Proc. Natl. Acad. Sci. USA 105 (2008) 15287–15292.
[33] J.M. Hayden, L. Brachova, K. Higgins, et al., Induction of monocyte differentiation and foam cell formation in vitro by 7-ketocholesterol, J. Lipid Res. 43 (2002) 26–35.
[34] J.X. Rong, M. Shapiro, E. Trogan, et al., Transdifferentiation of mouse aortic smooth muscle cells to a macrophage-like state after cholesterol loading, Proc. Natl. Acad. Sci. USA 100 (2003) 13531–13536.
[35] T. DeVries-Seimon, Y. Li, P.M. Yao, et al., Cholesterol-induced macrophage apoptosis requires ER stress pathways and engagement of the type A scavenger receptor, J. Cell Biol. 171 (2005) 61–73.
[36] C. Shi, X. Zhang, Z. Chen, et al., Integrin engagement regulates monocyte differentiation through the forkhead transcription factor Foxp1, J. Clin. Invest. 114 (2004) 408–418.
[37] F. Martino, E. Martino, M. Iacobini, et al., Down regulation of CD11b and CD18 expression in children with hypercholesterolemia: a preliminary report, Nutr. Metab. Cardiovasc. Dis. 19 (2009) 105–109.